DESIGN AND IMPLEMENTATION OF A SYSTEM FOR MEASURING AN AERODYNAMIC DRAG COEFFICIENT

A THESIS
SUBMITTED TO THE COLLEGE OF ENGINEERING OF AL-NAHRAIN UNIVERSITY IN PARTIAL FULFILLMENT OF THE REQUIREMENTS FOR THE DEGREE OF MASTER OF SCIENCE IN MECHANICAL ENGINEERING

By

Hyder Hassan Abd Husain

(B.Sc.2001)

Rajab **1425**
September **2004**

Certification

I certify that this thesis titled**“ Design and implementation of a system for measuring an aerodynamic drag coefficient”** was prepared by **Hyder Hassan Abd** under my supervision at Al-Nahrain University, College of Engineering, in partial fulfillment of the requirements for the degree of Master of Science in Mechanical Engineering.

Signature:

Name: **Dr.Adnan A. AL-Qalamchi**

Date: / / 2004

Signature:

Name: **Dr. Fawaz Abbas Al-Najim**

Date: / / 2004

Certificate

We certify, as an examining committee, that we have read the thesis titled "**Design and implementation of a system for measuring an aerodynamic drag coefficient"** and examined the student by **Hyder Hassan Abd** and found that the thesis meets the standard for the degree of Master of Science in Mechanical Engineering.

Signature:

Name:
Dr. Fawaz Abbas Al-Najim
(Supervisor)

Date: / /

Signature:

Name: Asst. Prof.
Dr.Adnan A. AL-Qalamchi
(Supervisor)

Date: / /

Signature:
Name:

(Member)

Date: / /

Signature:
Name:

(Chairman)

Date: / /

Signature:
Name:

(Member)
Date: / /

Signature:
Name:

(Chairman)
Date: / /

Approval of the College of Engineering

Signature:

Name:
(Dean of Engineering College)

Date: / /

Abstract

The research aims to design and construct a device to measure the drag coefficient for the free falling and accelerating bodies in different fluid mediums.

Four main factors are know to have an effect on free falling bodies. These factors are: shape, size density of the body and density of the medium through which the body travels.

In this study, spherical and cylindrical shape bodies were investigated. Carbon steel and glass spheres of diameter range (0.5-20 mm) were considered also carbon steel cylinders of l/d range (1.33, 1.375, 1.44, 1.54, 2.5, 3.33, 4) were investigated. Water and air media were used through which the falling bodies were allowed to drop.

The experimental results revealed that the speed of the falling bodies increases with displacement until terminal velocity is reached. This was true for both shapes and water medium and the experimental results were found to follow the theoretical ones with insignificant variation specially at low velocities.

Drag coefficient was calculated after the establishment of the terminal velocity for each body shape used in the case of free falling and hence the relation between drag coefficients and Reynolds number were determined.

The comparison between the practical and the theoretical results shows that the practical one is very close to the theoretical in the establishment of the terminal velocity. While the practical results related to the drag coefficient were very close to that obtained from the Reference [16].

Appendix A

Numerical Solution of Ordinary Differential Equation –Initial-Value Problems Using Runge-Kutta Methods

The numerical solution of initial-value problem that involve nonlinear ordinary differential equation is considered in this section. Where the Runge-Kutta methods were introduced for solving the first-and second –order equations. They are applied in this chapter for finding the motion of a free –falling sphere through air or any another fluid.

Considering the simplest case of a first-order ordinary differential equation having the general form

$$dx/dt = f(x, t) \qquad \text{a-1}$$

Where f is an analytic function. If at a starting point $t\text{-}t_0$ the function x has a given value x_0, it is desired to find x (t) for $t>t_0$ that satisfies both (a-1) and the prescribed initial condition. Such a problem is called an initial-value problem. To solve the problem numerically, the axis of the independent variable is usually divided into evenly spaced small intervals of width h whose end points are situated at

$$t_i=t_0+i*h,\ I=0,1,2\ldots \qquad \text{a-2}$$

The solution evaluated at the point t_i is denoted by x_i. Thus, by using a numerical method, the continuous function x (t) is approximated by a set of discrete values x_i, I=0,1…as sketched in fig (a 1). Since h is small and f is an analytic function, the solution at any point can be obtained by means of a Taylor's series expansion about the previous point.

$$x_{i+1}=x(t_{i+1})=x(t_i+h)=x_i+h(dx/dt)_I+h^2/2!*(d^2x/dt^2)+h^3/3!*(d^3x$$

$/dt^{3)}+\ldots$ a-3

$=x_i+h*f_i+h^2/2!*f'_I+h^3/3!*f''_I+\ldots\ldots$

Where f^n_i denotes d^nf/dt^n evaluated at (x_i, t_i). f is generally a function of both x and t, so that the first-order derivative is obtained according to the formula

$df/dt=\partial f/\partial t+dx/dt*\partial f/\partial x$ a-4

Higher-order derivatives are obtained by using the same chain rule.

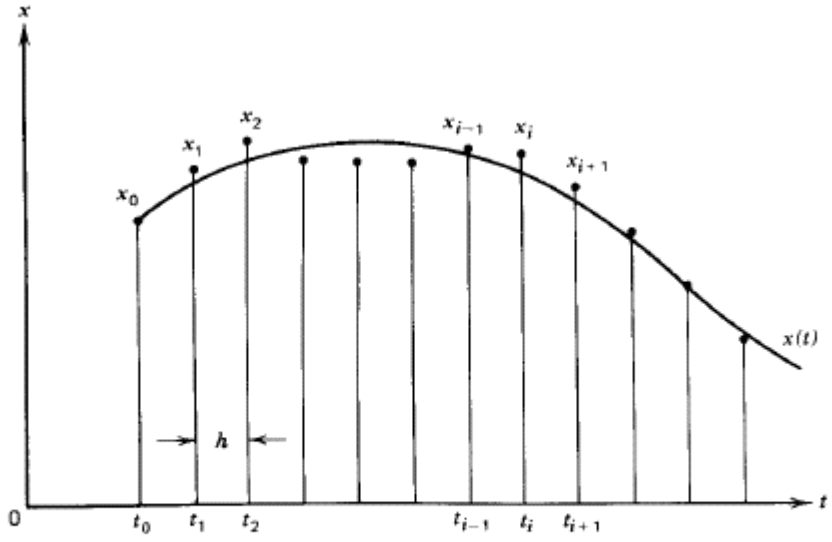

Figure a.1 Numerical solution of an ordinary initial-value problem.

Alternatively (a-3) can be rewritten as

$x_{i+1}=x_i+\Delta x_i$ a-5

Where

$\Delta x_i=h*f_i+h^2*f'_i/2!+h^3*f''_i/3!+\ldots$ a-6

Starting from I=0 with x_0 given and Δx_0 computed based on any desired number of terms in (a-6), the value of x_i is first calculated. Then, by letting=1,2,etc. in (a-5), the values of x_2, x_3, etc, are obtained successively.

Theoretically, if the number of terms retained in (a-6) increases indefinitely, the numerical result from this marching scheme approaches the exact solution. In reality, however, it is not permissible to do so, and the series has to be cut off after a certain finite number of terms. For example, if two terms are retained on the right-hand side of (a-6) in computing Δx_i, the value of x_{i+1} so obtained is smaller than the exact value by an amount $(h^3/3!)\, f''_I+(h^4/4!)\, f_i'''+\ldots$ .For small h the first term is dominant. We may say that the the error involve in this numerical calculation is of the order of the $h^3 f''_i$, or simply O $(h^3 f''_i)$. This is the truncation error that results from taking a finite number of terms in an infinite series.

It is termed Euler s method when only one term is used on the right-hand side of (a-6). The truncation error is O $(h^2 f'_i)$, and the method should not be used if accuracy is demanded in the result..

It is impractical to use Taylor's series expansion method if f is a function that has complicated derivative. Furthermore, because of the dependence of the series on the derivatives of f, a generalized computer program cannot be constructed for this method. The nth-order Runge-kutta method is a commonly used alternative. Computations in this method require the evaluation of the function, f, instead of its derivative, with properly chosen arguments; the accuracy is equivalent to that with n terms retained in in the series expansion (a-6). The second-order Runge-kutta formulas are

$$X_{i+1}=x_i+h*f\,(x_i+1/2*\,\Delta_1 x_i,\, t_i+1/2*h) \qquad \text{a-7}$$

Where

$$\Delta_1 x_i = h*f(x_i,\, t_i) \qquad \text{a-8}$$

For better results the following fourth-order Runge-Kutta formulas are usually employed:

$$X_{i+1}=x_i+1/6(\Delta_1 x_i+2\ \Delta_2 x_i+2\ \Delta_3 x_i+\ \Delta_4 x_i) \qquad \text{a-9}$$

In which the increments are computed in the following order:

$$\begin{aligned}
&\Delta_1 x_i = h*f(x_i,t_i)\\
&\Delta_2 xi = h*f(x_i+1/2*\ \Delta_1 x_i\ ,\ t_i+1/2*h)\\
&\Delta_3 x_i = h*f(x_i+1/2*\ \Delta_2 x_i\ ,t_i+1/2*h)\\
&\Delta_4 x_i = h*f(x_i+1/2*\ \Delta_3 x_i\ ,t_i+h)
\end{aligned} \qquad \text{a-10}$$

The derivation of these formulas can be found, for instance, in [29]. In the fourth method the dominant term in the truncation error is $(f^5/5!)\ f^{iv}$.

Unless the slope of the solution is very steep, satisfactory results are usually obtained with reasonably small h. Runge-Kutta methods can be extended to solving higher-order or simultaneous ordinary differential equations. Consider a second-order equation of the general form

$$d^2x/dt^2 = F(x,dx/dt,t) \qquad \text{a-11}$$

Accompanied by the initial conditions that $x=x_0$ and $dx/dt=p_0$ when $t=t_0$.by calling the first-order derivative a new variable p, the equation (a-9) can be written in the form of two simultaneous first-order equations

$$\begin{aligned}
&dx/dt=p\\
&dp/dt=F(x,p,t)
\end{aligned} \qquad \text{a-12}$$

With initial values $x\ (t_0) =x_0$ and $p\ (t_0)=p_0$. The fourth=order Runge-Kutta formulas for marching from t_i to $_{i+1}$are

$$x_{i+1}=x_i+1/6(\Delta_1 x_i+2\ \Delta_2 x_i+2\ \Delta_3 x_i+\ \Delta_4 x_i)$$

$$p_{i+1}=p_i+1/6(\Delta_1 p_i+2\ \Delta_2 p_i+2\ \Delta_3 p_i+\ \Delta_4 p_i) \qquad \text{a-13}$$

In which the individual terms are computed in the following order:

$$\Delta_1 x_i=h*p_i$$

$$\Delta_1 pi=h*F(x_i,p_i,t_i)$$

$$\Delta_2 x_i=h(p_i+1/2*\ \Delta_1 p_i)$$

$$\Delta_2 p_i=h*F(x_i+1/2*\ \Delta_1 x_i,\ p_i+1/2*\ \Delta_1 p_i,t_i+1/2*h) \qquad \text{a-14}$$

$$\Delta\ _3 x_i=h*(p_i+1/2*\ \Delta 2 p_i)$$

$$\Delta_3 p_i=h*F(x_i+1/2*\ \Delta 2 x_i,\ ½*\ \Delta_2 p_i,t_i+1/2*h)$$

$$\Delta_4 x_i=h*(p_i+\ \Delta 3 pi)$$

$$\Delta_4 p_i=h*F(x_i+\ \Delta_3 x_i,p_i+\ \Delta_3 p_i,t_i+h)$$

CHAPTER ONE

INTRODUCTION

1-1 GENERAL

For a relative motion between a body and a fluid ,as when a body moves through a fluid at rest or when a fluid flows over a body ,there are certain forces exerted on the body . The component of the force in the opposite direction of the relative motion is called drag force .Measuring this force has a variety of practical applications in the field of fluid mechanics for both internal and external flow. Different applications for external flow are the flow around aerofoil, flow around cylinders, wiers,sedimentation,or improvement of combustion and the minimaztion of erosion by droplets in large turbines.[1]

This drag force was found to depend on several factors including, the shape,alttiude, size of the body, the density and viscosity of the fluid. Also it depends on the velocity of the relative motion between the body and the fluid. Also the drag force depends on surface roughness of the body and the unsteadiness or turbulence in the fluid stream .

The drag force, at low velocities exerted between a solid body and a fluid flowing round it is due mainly to are pressure drag and the skin friction drag forces. As for the latter part is caused by the viscous shear forces in the boundary layers forming on the surfaces of the body . on the other hand, pressure drag is caused by the eddies forming in the wake of the body ,which cause eventually lower surface pressure and therefore resulting in drag forces .In Bluff bodies the major part of the drag is the

pressure drag .This creates interest in the investigation of the wake dynamics as the source of the pressure drag . The wake dynamics is reported to depend highly on the Reynolds number.

While the wake is steady for very small Reynolds numbers,laminar vortex shedding occures for intermediate Reynolds numbers ,and the wake becomes turbulent for high Reynolds numbers . Accordingly,the pressure drag varies depending on the wake dynamics.[27]

1-2 Streamlined and Bluff Bodies

A body is said to be streamlined if, when placed in a flow, the surfaces of the body tend to coincide with stream-surfaces. The streamlines, therefore, conform to the boundaries of the body. The boundary layer may commence at the leading edge but the layer grows from laminar to turbulent and does not separate until the trailing edge on a streamlined body. Consequently, there is none or little eddying zone and wake formation behind a streamlined body. However, A body may be streamlined at low velocities but not be so at higher velocities. And a body may be streamlined when placed in a flow in a particular direction but may not be so when placed in another direction. An example of streamlined body is a thin aerofoil when subject to a flow. Streamlined body experiences drag mainly due to the skin-friction at its surfaces. Normally, Streamlined bodies are employed to provide lift, i.e., force normal to the direction of the free stream. Since the drag on a streamlined body is low, the lift/drag ratio is high. Flight of birds is attributed to the production of high lift/drag ratio by virtue of wings attached to their bodies.

Mean while a body is said to be bluff if it requires the flow to turn suddenly subdivided it by separation at or near the leading edge. Thus, a bluff body may inhibit the formation of a boundary layer. The drag on a

bluff body is mainly due to the eddy-formation and wake effect. Bluff bodies are used to promote turbulence and mixing of flow with other substance and to accelerate diffusion in combustion chambers.

While a streamlined body is characterized by high skin-friction drag ratio, a bluff body is characterized by high form-drag to skin-friction drag ratio.[21]

1-3 Classification of Drag

When a fluid flows past a body immersed in it the following phenomena come into play:

Region (a): Divergence of streamlines with a consequent decrease in velocity and the occurrence of stagnation points up stream of the body, which divides the flow into two streams.

Region (b): Boundary layer flow; laminar boundary layer until a certain distance and turbulent boundary layer thereafter on the surfaces of the body.

Region(c): Separation of the boundary layers at one or more surfaces and rejoining of two streams at different velocities, resulting in a surface of discontinuity which breaks up to form vortices.

Region (d): Shedding of vortices behind the body to constitute the wake. The size of the wake is large if the separation takes place early in the boundary layer flow over the surfaces.

These phenomena are illustrated in fig (1) where the flow around the bridge pairs is sketched. The regions corresponding to the above phenomena are marked (a), (b), (c), and (d) respectively.

Consideration of the flow pattern around a body reveals that the fluid dynamic drag may be of different region. Formation of boundary layer and shear stresses at the surfaces in region (b) give rise to skin-friction drag. Formation of eddies and wakes in the region (d) result in pressure drag. The extent of pressure drag depends upon the body form of

the body. The pressure drag may far exceed the skin -friction drag for a badly designed or badly oriented body with respect to the flow. If a body is partly immersed in a liquid, the flow would include the formation of gravitational waves which result in wave-drag. On other hand, if the immersed body travels at transonic and supersonic speeds, the compressibility effect would give rise to wave-drag. The skin-friction drag and the form drag are generally taken together under a single name profile drag because both of them depend the profile of the body in relation to the direction of flow.

The drag due to three-dimensional nature of flow and finite size of a body is called induced drag. The induced drag is due to the induced component of velocity and vortices distribution along the span of the body. For instant, the induced drag on an aerofoil of a finite span depends upon the lift on the aerofoil as well as on the distribution of the lift over the span of the aerofoil.

Types of drag and their dependence on different factors are shown table (1).

The compressibility drag has its origin in the phenomena due to changes in density as the flow proceeds. At high speeds of flow, in the high subsonic range, boundary layers are thicker and grow faster due to compressibility effect. In supersonic flows, shock formation is accompanied by excessive energy loss. Further interaction of shocks wave may be formed. Thicker boundary layers and shock with boundary layers cause disruption of boundary layers and consequent excessive form drag. In hypersonic flows, the drag may practically stay constant. The effect of compressibility is different for different bodies. A cylinder would experience much more compressibility drag than a sharp- nosed projectile.

The gravitational wave drag is experienced by a body towed in a free surface flow or when a body is placed at the interface of air and a liquid. Under such conditions, the gravitational forces are of the same order as the inertia forces and hence the flow pattern is considerably influenced by the formation of gravitational waves. Surface waves are set up energy dissipation. Gravitational waves are formed ahead of, on the sides and at the rear ends of boats, ships.

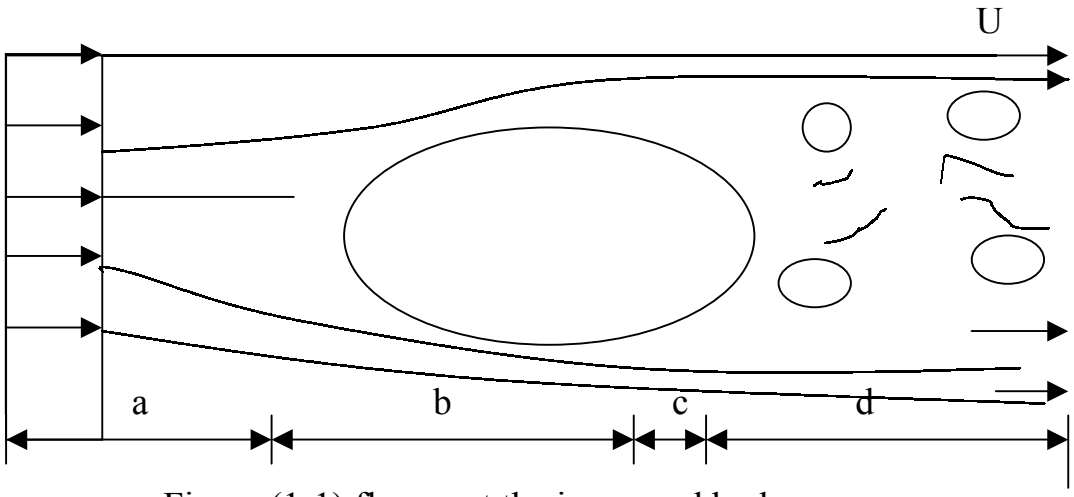

Figure (1-1) flow past the immersed body

CHAPTER TWO

LITERTURE REVIEW

2-1 General

The measurement of the drag coefficient has received considerable attention since the early days of the last century. Several mathematical models and experimental studies were carried out to estimate such coefficients for the measurement of several shapes against the flow of the two types of fluids. However, the development of mathematical model for estimating drag coefficient values is primarily based on measurement accuracy. The literature includes both theoretical and experimental studies. The drag coefficient may equally be measured in both Newtonian and Non-Newtonian fluids by using the terminal velocity provisions

2-1 Theoretical Studies

A .N. Pavlov, S.S. Sazhin, R. P. Fedorenko, M. R. Heikal [2] reported the detailed results of numerical calculations of transient, 2D incompressible flow around and in the wake of a square and cylindrical prism at Re =100, 200, and 500. They described implicit finite-difference operator-splitting method, a version of the known SIMPLEC-like method on a staggered grid. The method was found to have second-order accuracy in space, conserving mass, momentum and kinetic energy. As for the elliptic pressure problem, a new modification of the multigrid method was employed. Calculations were performed on a sequence of spatial grids with up to (401×321) grids points, at sequentially halved time steps to ensure grid-independent results. Three types of flow were

shown to exist at Re=500, a steady-state unstable flow and two transient fully periodic and asymmetric about the centerline but mirror symmetric to each other. Discrete frequency spectra of drag and lift coefficients were presented. On the other hand Arnal, M. P., Goering [3] reported the detailed results of numerical calculations of transient flow around a bluff body in 2D and 3D for (Re=100,500,1000). Calculations were performed on a sequence of spatial grids with up to (120*137) grid points using explicit Runge-Kutta approximation of momentum equation.

Chven-Yenchow [6] reported the special problem of incompressible flow past a sphere, where the Galerkin method was used to solve the Navier-stokes equation for Re =10,100, and 300 and calculate the drag coefficient. Streamline plots showed an almost fore-after symmetric flow pattern at Re=10. The expansion in the separated flow region as the Reynolds number increased from 100 to 300 was also seen.

Davis, H.W. and Moore, E.F. [9] and davi, R.W., E.F. and purtell, L.P. [10] reported detailed results of numerical calculations of transient flow around rectangular cylinders at Re=100,200,and 800. Calculations were performed on a sequence of grids (61*74). Using "QUICKEST" method. Kondo [24] reported his study about the flow around rectangular cylinders where the finite element method was used to solve the incompressible Navier-stokes equations and calculate the drag coefficient, at Re =10^4 with grids up to (1.4×10^4)

Li and Humphrey [25] showed the numerical results of flow around a square cross sectional cylinders with various orientations for (Re range from 100 to 1000) where explicit Runge-Kutta approximation of momentum equation in time was used, the number of staggered grids up to (100×55). Okajima et al. [30] Introduced the numerical results of comparison between laminar and turbulent flows around rectangular cylinders where (Re=$1,4,7\times 10^3$) approximation of momentum in space

and time method was used, and found that the laminar model provides more adequate results than the turbulent model. Xi [39] studied the flow around fins for different cross sections at Re=180,200. They used fully implicit approximation of momentum equation in time where the grid reached up to (380×130). Wissink [32] reported the use of the direct numerical simulation approach to predict some characteristics of two-dimensional turbulent flow at $Re=10^4$.

More over Zhng, and Balachander [38] Tackled numerically the problem of the fluid flow around three dimensional fin heat exchangers at the range of Re =18 to 750.

2.3 Terminal Velocity Measurement

The measurement of terminal velocity is used to measure the viscosity in a falling sphere viscometer, The measuring of the unknown viscosity system consists of a tall vertical transparent tube filled with fluid, provision is made to release and drop a spherical ball. After a short distance of travel, the ball acquires a constant velocity. The time to traverse a known vertical distance between two fixed marks on the tube is noted to calculate the terminal velocity U of the ball. The expression to determine the dynamic viscosity was obtained. [18]

Blake, R.W. [4], Gal, J.M. [14], Webb, P.W. [33] had reported that to generate a steady flow relative to an object or to move the object at a constant speed through a stationary fluid. In the laboratory a motor-driven translating table commonly generates this steady movement. However, steady movement through a stationary fluid also occurs when a falling object has reached terminal velocity; the object is no longer accelerating under the influence of gravity and its velocity remains constant with the further passage of time. The phenomenon of terminal velocity may be exploited to provide steady flow relative to an object for the purpose of estimating the drag within range velocities. This method is appropriate

for applications other than falling under the influence of gravity has been used to estimate drag on fish and frogs and it is used for drag measurement on slower or smaller object.

Clift, R., Grace, J.R.and Webber [5] had made development the 12 different empirical equation was listed all with ($0<Re<3*10^5$) for spheres and the other simple shapes.

CILOUDON and ZHANG [7] reported measuring the drag coefficient of spheres and simple shapes like antennae using terminal velocity method. The Reynolds numbers for the falling spheres ranged from 44to306. Individual spheres (3.175-mm diameter plastic spheres of 1138 kg m^{-3} density and 6.35-mm diameter glass spheres of 253kg m^{-3} density) were allowed to fall inside a Perspex box (0.15m$\times$ 0.11m$\times$0.20m high) filled with aqueous ethanol or glycerol solutions or water at temperature ranging from 18.2 to 26 c (depth of the fluid was 0.17m).

Falling objects were videotaped from the side using a Panasonic WV CL 1200 camera at standard speed (60 fields/s) in a horizontal orientation from a distance of a 2 m. The terminal velocity for any individual drop was estimated from the average velocity for the middle third of the 0.17 m fluid height in the tank. The results for the drag coefficients of the spheres estimated using theoretical equation were within 10% of the values predicted from theoretical equations. It concluded that the drag measured on single antenna using the terminal velocity assays were comparable in magnitude to drag measured on antenna using a different method in a wind tunnel.

Douglas [8] used terminal velocity method to graph the relation between ($C_d Re^2$) with (Re) where Re is the terminal Reynolds number at the terminal velocity for a simple shape like sphere.

G. Matijasl and A Glasnovic [13] measured drag coefficient of spheres, in non-Newtonian fluids where the evaluation based on the

mathematical equation is very significant. Development of mathematical model for estimating drag coefficient value is primarily based on measurement accuracy. The experiments were run using carboxymethylcellulose (CMC) aqueous solutions with different rheological properties that were determined by viscosity measurement. Approximately 200 experimental results were obtained using spherical particles of different materials and diameters. Measurements of its falling velocities were carried out in glass tube. An optical method of measurement was developed for this purpose.

Joseph [18], J.F. Douglas [17] showed the falling sphere viscometer used to measure the viscosity of many types of liquid for Re <1, where the terminal velocity of falling sphere was obtained from measurement.

J.S.Mcnown [19] discussed the effect of wall, the liquid is contained in a tube, the wall effect influence the drag force and hence the fall velocity. It has been found that the wall effect can be expressed approximately as

$$V/U=1+(9d/4D)+(9d/4D)^2$$

Where D is the tube diameter, and U represents the fall velocity in the tube .The above equation is reliable only if $d/D< 1/3$.

Thomoson and A.F.Kuckes [28] was estimated the viscosity of glycerin by measuring the velocity of a falling sphere. The velocity of the falling sphere can be measured by noting the time at which it moves through each of the four light beams. The essence of the following experimental work was to write programs in order to measure the required time and to graph the resulting data.

N. Mordant and J. F. Pinton [29] studied experientially the motion of a solid sphere settling under gravity in a fluid at rest, the particle

velocity was measured with a new acoustic method, It was based on the measurement of the Doppler shift of an ultrasonic wave scattered by the moving particle.

Variation of the sphere size and density allowed, measurements at Reynolds numbers, between 40 and 7000. Comparison of the dynamics of spheres of different densities for the same Reynolds number showed that the density is an important control parameter. Light spheres showed transitory oscillations at Re approximately 400, but reach a constant limit speed.

2-4 Scope of this Work

The measurement of the drag coefficient of any body through movement through fluid medium rests, for the fore seen future, of significant importance in experimental fluid mechanics.

Although the measurement of the drag coefficients using the wind tunnel dominated the field, the terminal velocity measurement in order to predict the drag coefficient device has its equal significance. In this work, a terminal velocity measuring device will be designed and constructed.

In order to assess the potential of this system, several experimental runs are to be carried out by the free falling of spheres and cylinders of several densities in water fluid mechanics. By measuring the terminal velocity, it is then compared to the theoretical results that were obtained by solving the equation of the free falling body using Runge-Kutta numerical scheme using already published drag coefficients. And experimental run is to be carried out by force falling of steel sphere. By measuring the velocities at three stages and then substitute in equation (3-11).

CHAPTER THREE

THEORETECAL WORK

3-1 Introduction

When a body is allowed to drop in a fluid, it acquires a velocity U such that it remains constant thereafter. For example, if a body is dropped, starting from rest, in the atmosphere it will accelerate under the action of its own weight, i.e., with acceleration due to gravity. As the speed of the body increases, the body will experience a drag force that tends to oppose the motion of the body. The drag force increases with the velocity of fall. At the terminal or equilibrium state, the upward drag force would just balance the downward weight force and the net force acting on the body would be zero. Under this state of no external force acting on the body, the body has no acceleration and hence it attains a constant velocity called the terminal velocity. The velocity of a falling body cannot be more than the terminal velocity. In other words, the terminal velocity is the maximum attainable velocity by a freely falling body in an environment.[21]

The concept of terminal velocity holds for a simple body such as a sphere or for a composite body such as a paratrooper together with the parachute. It may also be realized that the terminal velocity is low for high-drag bodies and high for low-drag bodies. At the instant the body has acquired the terminal velocity, the body must be in equilibrium, i.e., the net force on the body must be zero. The weight of the body, the drag force and the buoyancy force must add to zero.

3-2 Problem Formulation

This section is constructed to study the motion of the body falling in a fluid formulating the body motion, including the forces caused by the surrounding fluid, and then perform the numerical solution using Runge-Kutta method and then presented the associated computer program.

Because of the available drag data a cylindrical body was preferred as two-dimensional example, and a spherical body was preferred as three dimensional body examples.

The z-axis is chosen in the direction of gravitational acceleration g; its origin coincides with the center of the cylinder and sphere at initial instant t=0, assuming the cylinder is of diameter (d_l) and length (l_l) and mass (m_l) is at a distance z from the origin and has a velocity v, and the sphere is of the diameter (d) and mass (m) both are surrounded by a fluid of density ρ_f and kinematics viscosity υ.In vacuum the only external force acting on the body is the gravetential pull, mg, in the positive z direction. While moving through a fluid it is acted upon by the following additional forces:

1. The buoyant force, According to Archimedes principle, the buoyant force is equal to the weight of the fluid displaced by the body. It has the expression –mg, where

For a sphere $$m_f = (\pi / 6) d^3 \rho_f \qquad 3\text{-}1$$

For a cylinder $$m_f = \tfrac{\pi}{4} D^2 l \rho_f \qquad 3\text{-}2$$

Then $$F_b = m_f g \qquad 3\text{-}3$$

2. The force on an accelerating body. When a body immersed in a stationary fluid is suddenly set in motion, a flow field is induced in fluid. The kinetic energy associated with the fluid generated by moving the body against a drag force. This force is

$$F_h = -1/2 * m_f dv/dt \qquad 3\text{-}4$$

3. The force caused by viscosity. Around a body moving through a real fluid, a region of rapid change exists adjacent to the surface.[17]

$$F_d = 1/2 C_D A_l v^2 \rho_f \qquad 3\text{-}5$$

4. Wave drag. When the speed is comparable to the speed of sound in a fluid medium, shock waves may develop on or ahead of the body, causing a wave drag. However, for show free dropped body this force can be limited.

3-2-2 The Governing Equation

Applying the Newton's law of motion to a spherical body, moving at subsonic speeds the wave drag can be safely omitted [6], has the form

$$F_d + F_g + F_b + F_h = m\frac{dv}{dt} \qquad 3\text{-}6$$

Substituting from (3)(4)(5) becomes

$$m\frac{dv}{dt} = mg - m_f g - \frac{1}{2}m_f \frac{dv}{dt} - \frac{1}{2}C_D \rho_f v^2 A \qquad 3\text{-}7$$

So that the direction of viscous drag is always opposite to the direction of velocity . after rearranging, it can be written as

$$\left(m + \frac{1}{2}m_f\right)\frac{dv}{dt} = \left(m - m_f\right)g - \frac{\pi}{2}C_D \rho_f v^2 d^2 \qquad 3\text{-}8$$

For sphere $$m = \frac{\pi}{6} D^3 \rho \qquad 3\text{-}9$$

For cylinder $$m = \frac{\pi}{4} D^2 l \rho \qquad 3\text{-}10$$

The left-hand side indicates that in an accelerating or decelerating motion through a fluid, the body behaves as the added mass. Substituting equation (3-1) for falling sphere, and equation (3-2) for falling cylinder, and from equation (3-9) for sphere, and (3-10) for cylinder become

$$\frac{dv}{dt} = \frac{1}{A}\left[B - Cv^2 c_d\right] \qquad 3\text{-}11$$

with

$$\frac{dz}{dt} = v \qquad 3\text{-}12$$

$$\frac{dv}{dt} = v\frac{dv}{ds} \qquad 3\text{-}13$$

where

$$\bar{\rho} = \frac{\rho_f}{\rho} \qquad 3\text{-}14$$

For sphere

$$A = 1 + \frac{1}{2}\bar{\rho}$$

$$B = \left(1 - \bar{\rho}\right)g \qquad 3\text{-}15$$

$$C = \frac{3\bar{\rho}}{4d}$$

For cylinder $A = (1 + \frac{1}{2}\bar{\rho})$

$$B = (1 - \bar{\rho})g$$
$$C = \frac{2\bar{\rho}}{\pi D} \qquad \text{3-16}$$

These equations fit the general form (3-29) and can be solved by applying Runge-kutta method, however in the following section the equation (3-7) will be solved to find a term for the terminal velocity where the case of no memory was considered [27].

3-2-3 The Terminal Velocity

When a body traveling at the terminal velocity, the gravitational force is balanced by the sum of buoyancy and viscous drag, so that the acceleration is zero. From equation (3-8) an expression is derived for the terminal velocity

$$V_t = \frac{2mg(\rho - \rho_f)}{A_l \rho C_D \rho_f} \qquad \text{3-17}$$

3-3 IMPERCAL Values Of Drag Coefficient

A-The sphere

For numerical computation, we need an empirical value for the drag coefficient c_d. To present it in a form suitable for the computer computation, the general published curve [6] for a sphere is replaced by several broken lines, as shown in Fig (3-1) .

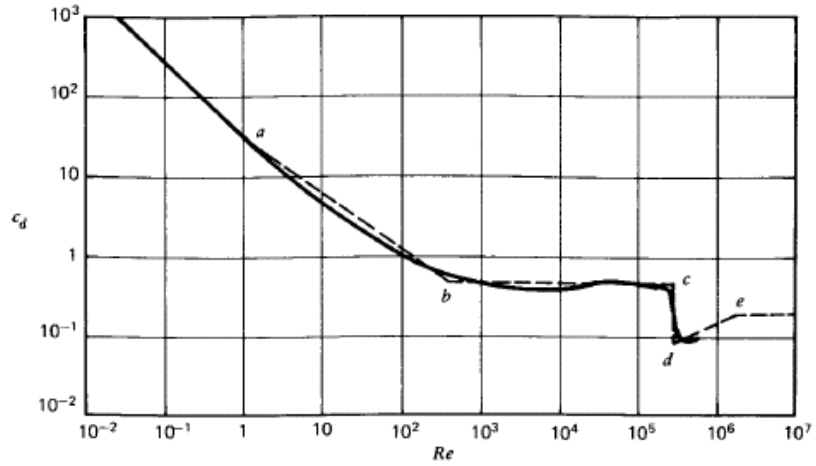

Figure 3.1: Empirical drag coefficient of sphere [6]

To the left of the point a, where Re<1, the Stokes formula

$$c_d = \frac{24}{\mathrm{Re}}$$

is used, which coincides well with the experimental curve for Reynolds numbers that are much less than unity and deviates only slightly from it in the neighborhood of the point a (where Re=1,c_d=24).On the log-log plot a straight line is drawn between points a and b(where Re=400,c_d=0.5)to approximate the actual curve, which gives

$$c_d = \frac{24}{\mathrm{Re}^{0.606}} \qquad \text{for} \quad 1<\mathrm{Re}<400$$

Between b and c (where Re=3x10^5), we assume that the drag coefficient has a value of 0.5. The abrupt drop of drag coefficient around c is an indication of transition from laminar to turbulent boundary layer before flow separates from the body surface.

Another straight line is drawn between d (where Re=3*10^5,c_d=0.008) and e (where Re=2*10^6,c_d=0.18). Thus

$$c_d = 0.000366 \times \mathrm{Re}^{0.4273} \qquad 3 \times 10^5 < \mathrm{Re} \le 2 \times 10^6$$

Finally in the high Reynolds number region beyond e, a constant value of 0.18 is assumed for the drag coefficient.

B-The cylinder

For the numerical computation, In a similar manner to the sphere computation defining the value of the drag coefficient C_d the empirical functions of a cylinder.

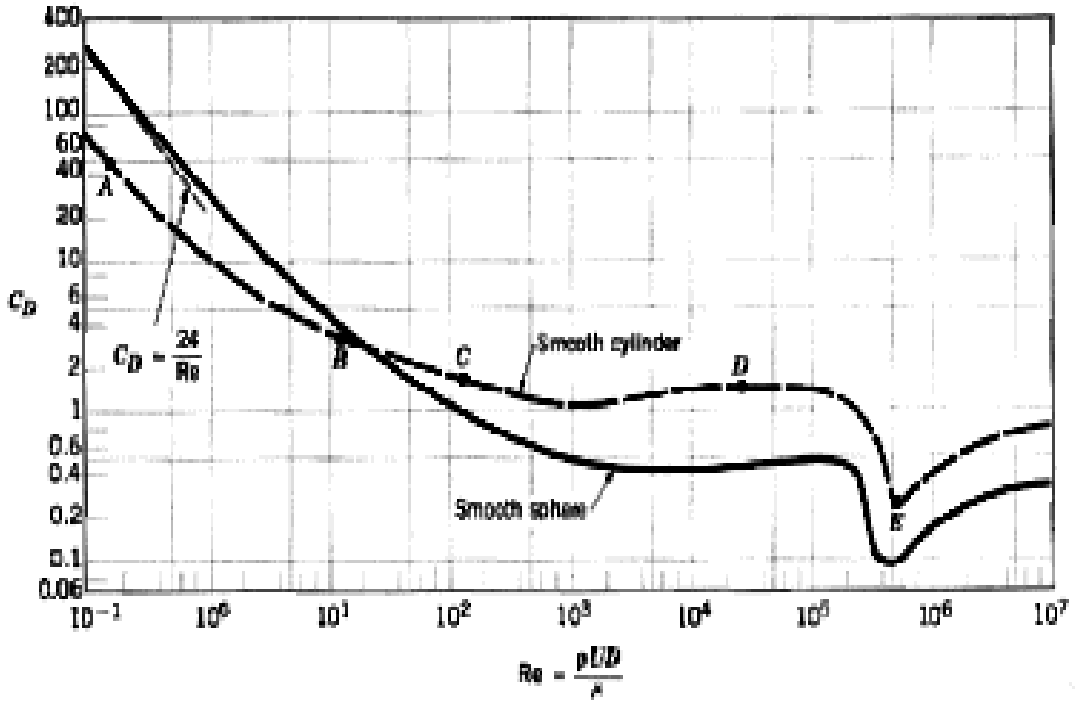

Fig 3.2: Drag coefficient for smooth cylinder and sphere[21].

Between a and b

$$c_d = \frac{2.388}{\mathrm{Re}^{0.748}} \qquad 0.1<\mathrm{Re}<10$$

between b and c

$$c_d = \frac{1.624}{\mathrm{Re}^{0.223}} \qquad 10<\mathrm{Re}<2000$$

For Re between c and d the drag coefficient may be approximately constant (c_d=1.1), and for Re between d and e

$$c_d = 6.293 \times \mathrm{Re}^{0.359} \qquad 2\times10^5 \le \mathrm{Re} \le 2\times10^6$$

Finally, in the high-Reynolds number region beyond e, a constant value of 0.7 is assumed for the drag coefficient.

CHAPTER FOUR

EXPERIMENTAL WORK

4-1 GENERAL

The experimental work associated with the scope of this work includes the construction of a system to measure the drag coefficient. By measure the velocity of the falling bodies (spheres, cylinders) either accelerated or freely through a fluid medium .

This system includes the following

4-2 Experimental set-up

4-2-1 fluid medium holders

A square cross sectional glass tube (11×11) cm cross-section was chose to avoid the effect of boundary layer also to give the ability for the working of IR Transmitter Receiver, Also the length of tube (2 m). Open from one end and closed from the other, the thickness of the glass is 6 mm. Enabling the fixing of the holders and the IR Transmitter and Receiver on the opposite sides of the walls near the closed end, a top was fixed to allow changing the fluid filling the tube as shown in fig (4-1).

4-2-2 The Velocity Measuring Unit (Chronograph)

The basic criterion of the velocity-measuring unit is to measure the time interval that takes the body to cross a pre-determined distance.

Figure (4-2) shows the general shape of the circuits while Figure (4-3) shows a block diagram of the unit that has provisions for the measurement of the velocity.

Evidently, the unit consists of three identical measurement groups; each group is integrated from the following elements:

1. IR Transmitter circuit and IR Receiver circuit

The Infra Red Transmitter (IR) sends out Infra Red rays, the IR Receivers sensed these rays. When the moving body passes by the IR Transmitter and the opening Receiver rays are cut. Consequently, the IR Receiver circuit gives a signal to the counter circuit to start country the time elapsed before the body reaches the next IR Transmitter-Receiver couple positional at a predetermined distance. Figure (4-4) shows the IR Transmitter circuit while fig (4-5) shows the IR Receiver circuit.

2. Signal processing circuit, figure (4-6) shows the electronic circuit used for processing the electrical signal that is generated as the body cuts off the rays between the line of IR Transmitter and the opposing IR receiver as it passes through them. The electrical " pulse" of the first line sensor and receiver is filtered and amplified through a flip-flop integrated circuit to trigger on the time counting circuit. The second "pulse" is generated as the body passes through the second line of IR Transmitter and IR Receiver. This "pulse" is manipulated in the same way, and it is used subsequently to stop the time counter.
3. Electrical Digital Clock Circuit a (1 MHz) crystal quartz oscillator generates a series of equally timed pulses; these pulses are further fed to a (DIP) switch speed selector, through a series of digital gates, in order to obtain a wide range of frequencies ranging from 500 to 16 kHz according to the desired accuracy.
4. Electronic Time Counter / Display Circuit, kept fed by the electronic clock pulses, the output signal of the signal processing stage that results as the body passes through the first line of IR Transmitter and IR Receiver starts the counting.

Subsequently, the second signal that results as the body reaches the second line of the IR Transmitter and IR Receiver stops counting.

The same sequence of events is repeated as the body passes through the following IR Transmitter-Receiver couples. Finally, the elapsed time between each two consequent events is displayed on the seven-segment screen.

Figure (4-7) shows a detailed diagram of the electronic signal at each stage.

Basically, dividing the distance between two consecutive IR Transmitters-Receiver couples by the time needed to cross it may obtain the body velocity.

4-2-3 Holders of the IR Transmitter and receiver

The holders were used to set the IR Transmitter-Receiver couples a fixed in position around the glass tube. Each holder made from (2 mm) steel plate joined around the vertical tube using (M4) bolts holes were drilled at predetermined positions where the Transmitter and receiver couples are fixed using silicon adhesive.

Figure (4-8) show Four plates were set for each line of IR Transmitter and receiver.

4-2-4 The Properties of the moving objects

The bodies used in the course of this work were made of steel and glass. The solid spheres of different diameters and cylinders with different diameters and lengths as appearing in tables (4-3) and (4-4) were used.

4-3 Body Accelerating Device

As previously mentioned, the system was designed to measure the velocity of free falling or accelerated bodies. The provisions for accelerated movement of bodies consisted powder powered launching device capable of accelerating (7.9 mm) diameter spheres and cylinder to velocities up to 400 m/s.The device consisted of a smooth bore gun barrel

of (7.9 mm) nominal internal diameter and (480 mm) length giving a length to diameter L/D ratio of approximately (61). The smooth bore enabled the use of the gun to propel rigid projectiles of any shape. Moreover, the cartridge housing situated at the rear end of the gun was constructed so as to accommodate many kinds of powder gun cartridges. This capability enabled accelerating the projectiles to velocities ranging from (100 m/sec) to (900 m/sec). Finally, the materials and dimensions were chosen so as to withstand internal pressures as high as (3000 Bars) resulting from the detonation of the powder gun charge. Figure (4-9) is an assembly drawing showing the following basic parts:

a) The gun barrel: A long cylinder made of a special treated alloy steel with (27 mm.) outer diameter and (7.85 mm.) bore, one of the barrels ends was threaded externally to be fastened to the envelop housing.
b) The cartridge envelops: A steel cylinder of (27-mm.) outside diameter and (55 mm.) length, the inside configuration was machined so as to envelop the two types of cartridges used in this work.
c) The envelope housing: A hollow steel structure with an internal thread at one end through which it is fastened to the gun barrel. The other end is specially designed to be securely joined to the breech while the inside bore holds the cartridge envelops.
d) The breech: Made to be joined to the envelope housing at one end and to carry the firing pin at the other.
e) The firing: Two basic types of firing pins are used. One with a pointed head configuration suited for the capsule initiated cartridge, the other with a screw-drive head configuration suitable to the commercial type cartridges.

The launching device was mounted vertically on top of the glass tube as appearing in fig (4-10). And was filled in place by specially designed clamps.

4-4 Experimental Procedures

1. Calibration of the system.
2. Weight the cylinders and spheres and measure the all dimensions. Several spheres made of steel and glass and of geometrical dimensions as shown in table (4-3) while steel cylinders geometry and dimensions shown in table (4-4).
3. Holders of the IR transmitters and receivers were set pre-design in positions.
4. The time counter was reset and the readings of the seven segments read out were set to zero.
5. The tube was filled by water.
6. The temperature of the laboratory was checked and was recorded.
7. The density of the water was determined from the tables at this temperature.
8. The body was then set to fall in the tube considering the fall to be among the line of transmitter receiver couples.
9. The time was recorded and the procedure was repeated three times then average reading for three measurements was considered and the velocity was calculated as shown in the sample of calculation.
10. The drag coefficient was computed through substituting the measuring velocity in equation (3-17).

Sample of calculation

The sphere of steel has 0.006 m diameter and mass of 7.24 g falling in water was taking as an example of calculation. The determination of average of reading and calculate the time is the first step in this calculation and then must be take the distance for each stage then calculate the velocity of sphere at all stages.

As shown in table (4-1) calculate first the average time recorded from the seven segments as shown in equation below

$$T_{ave} = \frac{T_1 + T_2 + T_3}{3}$$

And then convert the reading in seven segments to the time in second, and divided the distance on the time, as shown in table.

So from circuit of frequency divider as shown in figure (4-6) the Q_2 was taking as reference in free falling which equal to (0512e-3) sec.

Where for each stage

$$t = 0512 \times 10^{-3} \times T_{ave}$$

In this case the distance between each line was shown in table (4-1).

The velocity of free falling body can be obtained by dividing the distance by the time where

$$V(m/\sec) = \frac{dis\tan ce(m)}{time(\sec)} = \frac{S}{t}$$

And the density of the sphere

$\rho_b = \frac{m}{V}$ $\rho_b = \frac{m}{U}$, Where $V = \frac{4}{3}\pi R^3$

V=(4/3) π*(0.006)^3=0.000000904 m^3

ρ_b=0.00724/0.000000904=8001.9 kg/m^3

Table (4-1) specification of 0.006 m sphere falling in water .

Number of stage	Time Record T (0.512e-3) sec	Average recording for time. T_{ave}	Time in sec	Distance S m	Average velocity m/sec
I	169	170.33	0.0877	0.1	1.139
	171				
	170				
II	171	171.33	0.08772	0.1	1.1399
	172				
	171				
III	171	171.33	0.087722	0.1	1.1399
	172				
	171				

From equation (3-17) when substitute the terminal velocity as the velocity obtained in stage three where the body reaches the terminal velocity, and the all properties of water was taken from Reference [21]. and from the above equation the drag coefficient was obtained (0.4325).

Calibration of the system

The IR transmitters and receivers were checked for proper performance. The method adopted is to measure the velocity of a free falling body at two positions. A solid sphere of diameter 0.006 m and 7.24 g weight was dropped three times and the velocities were recorded. To calculate the acceleration of gravity (g) the following equation recommended by Reference [20] was used

$$V_2^2 = V_1^2 + 2gs \qquad 4\text{-}1$$

Where s is the distance between the two positions at which velocity measurement was made. The measured velocities at two positions and the distance between these two positions are listed in table (4-2). Equation (4-1) have yielded that the acceleration of gravity (g=9.82176) is very closed to that published for Baghdad of (34 m) elevation.

Table (4-2) velocity of 0.006 m sphere in air .

Stage of velocity	Record time (0.512e-3) sec	Calculated average time in sec	Distance of stage S in m	Velocity V m/sec
I	122	122.0	0.1	1.6
	122			
	123			
II	43	43.8	0.1	4.454
	44			
	44			

SubstitutethV$_1$, V2 from table (4-2) into equation (4-1)

$$g = \frac{(4.454)^2 - (1.6)^2}{2 \times (0.88)} = 9.817 \quad [\text{m/sec}^2]$$

Results Of Experimental Work

Free Falling Body

The table (4-4) shows the characteristics of solid spheres body and have experiments.

Where the column one is the diameters of the spheres, the second column is the types of material, the third column is the density of the body, the fourth column is the velocity of the third stage (terminal

velocity), the fifth column is the Reynolds number for the third stage of the falling spheres, and the sixth column is the drag coefficient of spheres.

In this determination the properties of water was taken from tables at the laboratory temperature and its equal (25 C), which obtained from measurements in laboratory.

Table (4- 3) Numerical Results of Experimental Work for Solid Spheres.

Diameters of the spheres d (mm)	Types of material of spheres	Density of the spheres ρ_b	terminal velocity (m/sec)	Reynolds number Re	Measured Drag coefficients of spheres C_D
0.5	glass	2560	0.0711	41	2.067
1.5	glass	2565	0.217	360	0.668
2	glass	2480	0.261	600	0.582
17	glass	2040	0.757	14346	0.413
20	glass	2200	0.8418	18773	0.416
0.8	Steel	7699	0.316	281	0.718
1	Steel	7850	0.383	427	0.624
2	Steel	8096	0.636	1418	0.469
3	Steel	8150	0.796	2662	0.453
4	Steel	8200	0.930	4147	0.445
6	Steel	8001	1.1399	7624	0.4325
8	Steel	7833	1.319	11763	0.42
12	Steel	7800	1.627	21765	0.412
15	Steel	7300	1.775	29682	0.4013

Table (4-4) Numerical Results of Experimental Work for Solid Cylinders.

Diam	Lengt	Type	Density	Terminal	Reynolds	Drag

eter d mm	h l mm	of materi al	Kg/m^3	Velocity m/sec	number	coefficient C_D
7	18	Steel	8228	0.898	4138	0.988
7	28	Steel	8166	0.902	4239	0.97
8	11	Steel	8247	0.856	4508	0.971
9	13	Steel	7860	1.07	6339	0.973
13	20	Steel	7910	1.18	10270	1.016
15	20	Steel	7922	1.27	12541	1.018
1.8	6	Steel	7800	0.31	391	1.78

Accelerating Body

The results for accelerating falling of sphere and cylinder was illustrated in table (4-5) where the velocity at two stage was measured and the distance between the center of these stages was given also density ratio was determined, so these magnitudes substituted into equation (3-11) after substitute the term of accelerating by equation (4-13).

Table (4-5) Numerical Results for accelerating bodies falling in air.

	Size of the body mm	Mach at stage one	Mach at stage two	Density of the body	Drag coefficient C_d
Sphere	D=7.9	0.53	0.6	8100	0.412
Cylinder	D/l=0.395	0.573	0.691	7805	0.53

CHAPTER FIVE

RESULTS AND DISCUSSION

5-1Introduction

In this chapter, the results of both the experimental work and those obtained from the theoretical model are presented, discussed and compared. Through the comparison made, the performance of the experimental rig that was designed and constructed during the course of this work is assessed.

5-2 Theoretical results

Two forms of falling objects, namely the sphere and the cylinder are chosen to carry out the theoretical computations. The theoretical model that was previously presented in chapter three is to be examined for the free falling and the initially accelerated body motion in fluid medium.

5-2-1 Effect of shape and geometry

Figures (5-1) and (5-2) show the relation between the velocity and time for falling steel spheres of diameters (0.006,0.008,0.012,0.015,0.7) m in air. The density of steel (8000 kg/m^3) and the density of air was taken from Ref. [19]. As shown in the figures above the falling spheres velocity increases from zero until it reaches the terminal velocity, which is seen to increase, with the diameter of the spheres. For smaller sphere, the Reynolds number is relatively low and the boundary layer always remains laminar before the point of separation. At a sufficiently high Reynolds number, when a transition from a laminar to a turbulent boundary layer occurs on a larger sphere, the abrupt decrease in drag shown in fig (3-1) will suddenly accelerate the sphere. As observed in fig (5-2) on the curve for a sphere with d=0.07m around t=6.2 s. For spheres of this diameters and larger the effect of the surrounding fluid

becomes negligible in comparison with body inertia, so that the sphere behaves as if it were moving in a vacuum. In this case the velocity increases indefinitely with time, and a terminal velocity can never be reached.

Fig (5-3) shows the relation between the velocity and the time for the steel cylinders falling in water. The selected cylinder diameters are (0.001,0.003,0.005,0.007) with a common length of cylinder 0.01. So the increase in diameter means the increase in Reynolds number the most influential parameter in flow around the cylinders.

The value of the terminal velocity and the time it takes to achieve depend on the diameter and the shape of the falling bodies. The time needed to reach the terminal velocity for a falling body depends on the size and the shape. The body of large diameter reaches the terminal velocity before the smaller and the cylinder reach its terminal velocity before the sphere because the drag for cylinder is greater than that for a sphere at the same Reynolds number. Yet for the same mass of a sphere and a cylinder falling and the same diameter the velocity of sphere is greater than the velocity of the cylinder.

5-2-2 Density effect

The density ratio $\bar{\rho} = \frac{\rho_f}{\rho}$ may be effective in terms (A, B, C) in equations where

For sphere $A = 1 + \frac{1}{2}\bar{\rho}$

$B = \left(1 - \bar{\rho}\right)g$

$C = \frac{3\bar{\rho}}{4d}$

and

For cylinder $A = (1 + \frac{1}{2}\bar{\rho})$

$$B = (1 - \bar{\rho})g$$

$$C = \frac{2\bar{\rho}}{\pi D}$$

The increase of density ratio increases (A), increases (C) and decreases (B) that means any increase in density ratio will decrease the acceleration of the falling body according to equation (3-11). The density ratio may be increased by increasing the density of the fluid medium this effect appear in figure (5-4) where the steel sphere falling in air need to (25 sec) to reach the terminal velocity while the same sphere falling in water needs to reach the terminal velocity approximately (3 sec), only because of the decrease in acceleration of the falling sphere. Eventually the decrease in density of a falling body increases the density ratio. Figure (5-5) show the relation of a falling 0.015 m glass sphere in air when compared with figure (5-1), the terminal velocity was reached for steel sphere with the same diameter at approximately 25 sec while for glass sphere it is reached in 8 sec. Also the magnitude of the terminal velocity for the steel sphere is 21 m/sec while for glass sphere is 2 m/sec. Figures (5-6), (5-7) shows the relation of velocity for falling steel spheres in water of properties from Reference [19] with time. The diameters of spheres were (0.0008,0.001,0.002,0.003,0.006,0.008,0.012,0.015) m and all shows the same trends.

5-2-3 Effect of initial velocity

Figure (5-8) show the relation of velocity with time for falling steel spheres in air with initial velocity 5m/sec, 15 m/sec. The velocity value of the sphere is seen to decrease until it reaches the terminal velocity. As for falling

bodies that have velocities less than its terminal velocity the velocity increases until it reach the terminal velocity, as for a falling body with an initial velocity greater than its terminal velocity the velocity of the body decreases until reach the terminal velocity of the body. Consequently the terminal velocity does not depend on the initial velocity.

5-3 Experimental Result

The measured terminal velocities are given in table (4-3) for spheres and table (4-4) for cylinders. In each case the motion has reached a stationary state, so that the terminal velocity is well defined. All the measurements present the mean value of the velocity obtained after averaging three readings of time. The drag coefficient was calculated by substitution in equation (3-11). In the calculation of Reynolds number, the physical properties appearing in Ref.[19] was used at temperature 25 °C for water a value confirmed by independent measurement with a chronograph viscosimeter.

The figures (5-9) show the experimental curve C_D versus (Re) for a range of Reynolds number from (10 to 30000). The results show good agreement. The drag coefficient was the same in the case of a fixed sphere measuring in wind tunnel and in the case of a free falling body when the experimental results was compared with the standard empirical drag measurements [16]. It is generally admitted this should be true at low Reynolds number, where the numerical and analytical studies agree that the drag is indeed given by the Stokes expression. However, at higher Reynolds this result is not obvious. Indeed, it may be surprising that the particle reaches a stationary terminal velocity, and thus probably stationary momentums flux across the wake. This is an important difference with observations of the wake past a fixed body where the incoming flow is set at a constant uniform speed and the force acting on the body may take any value. In that case, instabilities in the wake were known to exist and were related to vortex

shedding. In case of free falling, the constraint is just that the forcing gravity is constant; any change on the force felt by the sphere must be related to a change on the fluid motion.

Figure (5-10) shows the relation between drag coefficient and Reynolds number for falling cylinders in water and compared to the empirical data given in Reference [21]. The measured drag coefficients for the cylinders falling in water with range of Reynolds (391 to 18565). The drag coefficient of the cylinder is larger than the drag coefficient of spheres.

At Reynolds number 30 two symmetrical eddies, rotating in opposition to one another, are formed. Further increase of Re tends to elongate the fixed eddies, which then begin to oscillate until at Re=90, depending upon the free-stream turbulence level, the eddies being washed away by the main stream, this process is intensified by a further increase of Re, where by the shedding of eddies from alternate sides of the cylinder is continuous, thus forming in the wake two discreet rows of vortices. This is known as Vortex Street or von Karman Vortex Street. At this stage the contribution of pressure drag to the profile drag is about three quarters. Von Karman showed analytically, and confirmed experimentally, that the pattern of vortices in a vortex street follows a mathematical relationship,

$$(h/l) = (1/\pi)\sinh^{-1}(l) = 0.281$$

Where h is the distance between two eddies in two lines and l is the distance between two eddies in the same line. It was seem that shedding of each vortex produces circulation and, gives rise to a lateral force on the cylinder. Since these forces are periodic following the frequency of vortex shedding, the cylinder may be subjected to a forced vibration.

The frequency of such forced vibration, sometimes called self induced vibration, may be calculated from an empirical formula due to Vincent Strouhal $\frac{fd}{U} = 0.198(1 - \frac{19.7}{\mathrm{Re}})$

In which

$$Str = \frac{fd}{U}$$

and is known as Strouhal number. The formula applies to $250 < \mathrm{Re} < 2 \times 10^5$

There is a great similarity in the development of drag at increasing Re between the sphere and cylinder, except that the vortex street associated in two-dimensional bodies as in cylinders was not formed in the case of three-dimensional bodies as in sphere.

In the case of accelerating body the drag coefficient was measured at (M= 0. 569) for sphere was (C_D=0.412) and for cylinder at (M=0.5145) (C_D=0.53) so this result have difference when it compared with the results on Ref. [18]. These difference may be due to the average velocity was taken on the measurements of v_1, v_2 and not local velocity. From the other side the wave drag was canceled in equation (3-11) this decreases the drag coefficient. Where the acceleration of the sphere greater than that for cylinder also the velocity of sphere larger than the velocity of cylinder because the drag of sphere less than the drag of cylinder for the same diameter.

5-4 Comparison of experimental and theoretical results

Figure (5-11),(5-12)and(5-13) shows comparison between the experimental and theoretical results for the velocity of falling steel spheres in water with displacement where the theoretical result its approximately less than the experimental results, the difference for large sphere at the first stage may be due to the velocity measured it's the average velocity the difference was appear and for the small sphere when its reach the terminal velocity from

the first stage no difference between the average velocity measured and the local because the velocity was always constant.

Figure (5-14), (5-15) and (5-16) shows the relation between the displacement and the velocity with comparison between theoretical and experimental for a falling cylinder in water. Where the results for the experimental it's approximately less than the results of the theoretical work, and it’s a very close to it.

CHAPTER SIX

CONCLUSIONS AND RECOMMENDATIONS

6-1 CONCLUSIONS

From the results of the current research, the following notations can be stated on the operation of the experimental system and the various parameters affecting the motion of the bodies falling in fluids.

1. The measurements of velocity were average velocity in all cases but when the body reaches the terminal velocity the local velocity become equal to average velocity.
2. The terminal velocity was obtained from experimental was very close to the terminal velocity was obtained in theoretical model and very close to result given in Ref.[27]
3. The determination of drag coefficient from the measured terminal velocity was very close to the drag coefficient in Ref.[16].these give the surety to the system.
4. For the measurement of drag coefficient at high velocity depends on the M number and the measurement gives approximately high difference.
5. The velocity of the falling body increased with the time increasing until it reached the terminal velocity.
6. The terminal velocity depends on the density ratio $\overline{\rho} = \frac{\rho_f}{\rho}$.
7. Also the terminal velocity depends on the shape of the body where the terminal velocity of cylinder greater than the terminal velocity of sphere.

6-2RECOMMENDATION

1. Improve the sensors and the electrical circuit to measure the local velocity with time.
2. Increase the length of the tube to measure the terminal velocity for larger spheres.
3. Measure the drag coefficient in different fluid medium.
4. Improve the accelerating system to use for measuring deferent shapes.

NOMENCLATURE

1-Simple Variables:

Symbol	Definition	Units
C_D	Drag Coefficient	-
d	Diameter of the falling body	m
F_b	Bouncy force	N
F_d	Drag force	N
g	The acceleration of gravitational	W/m^2
l	Length of the cylinder	M
m_f	Mass of the moving fluid	Kg
m	Mass of the falling body	Kg
Re	Reynolds Number	-
s	Distance between two stage	m
t	Time	sec
V	Volume	m^3
v	Velocity	m/s
Vi	Velocity at stage	m/s
V_t	Terminal Velocity	m/s

3- Greek Symbols:

Symbol	Definition	Units
$\overline{\rho}$	Density ratio	-
ρ_f	Density of fluid	Kg/m^3
ρ	Density of the body	Kg/m^3

Contents

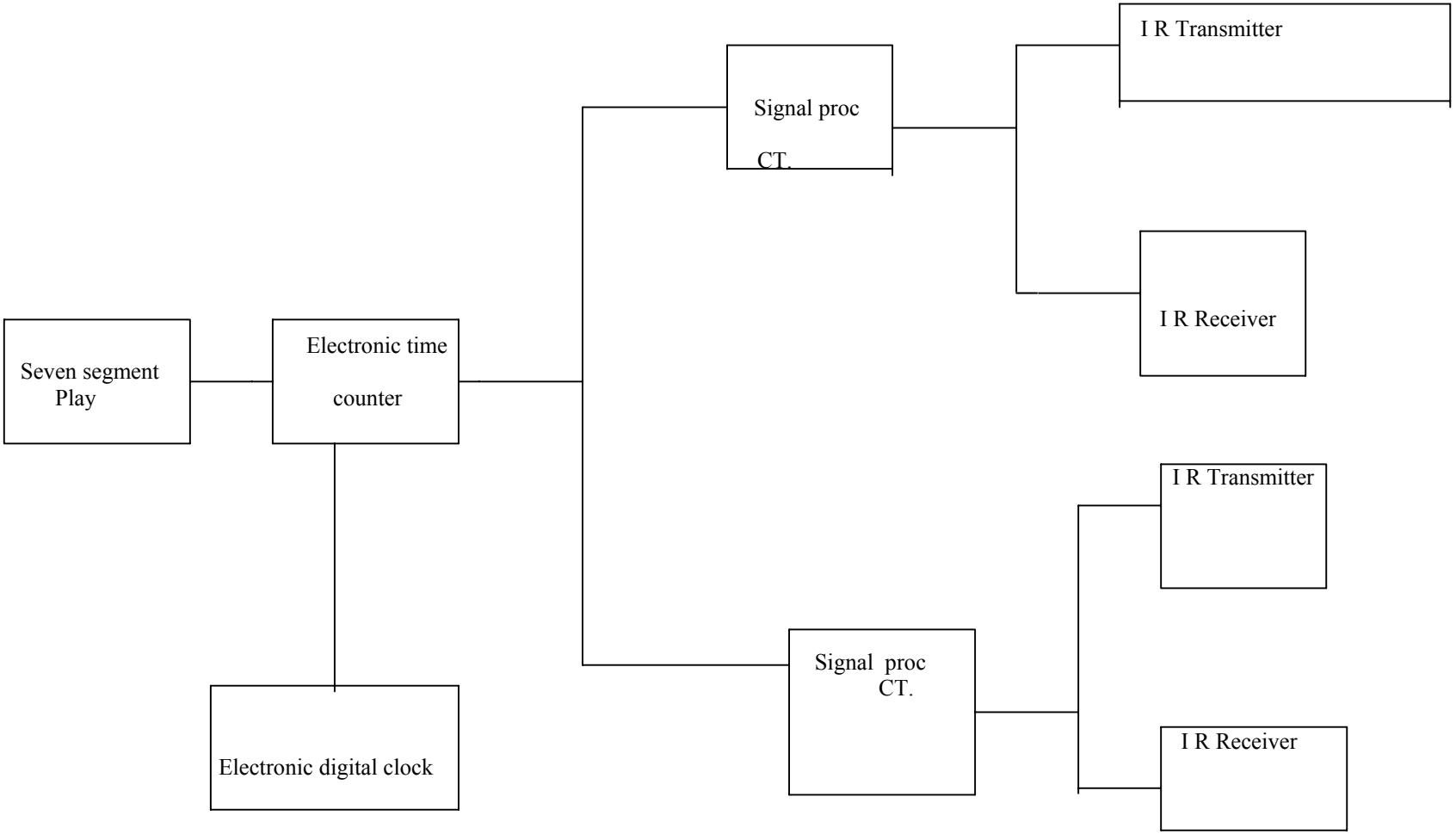

Figure (4- 3) block diagram of the velocity measuring unit.

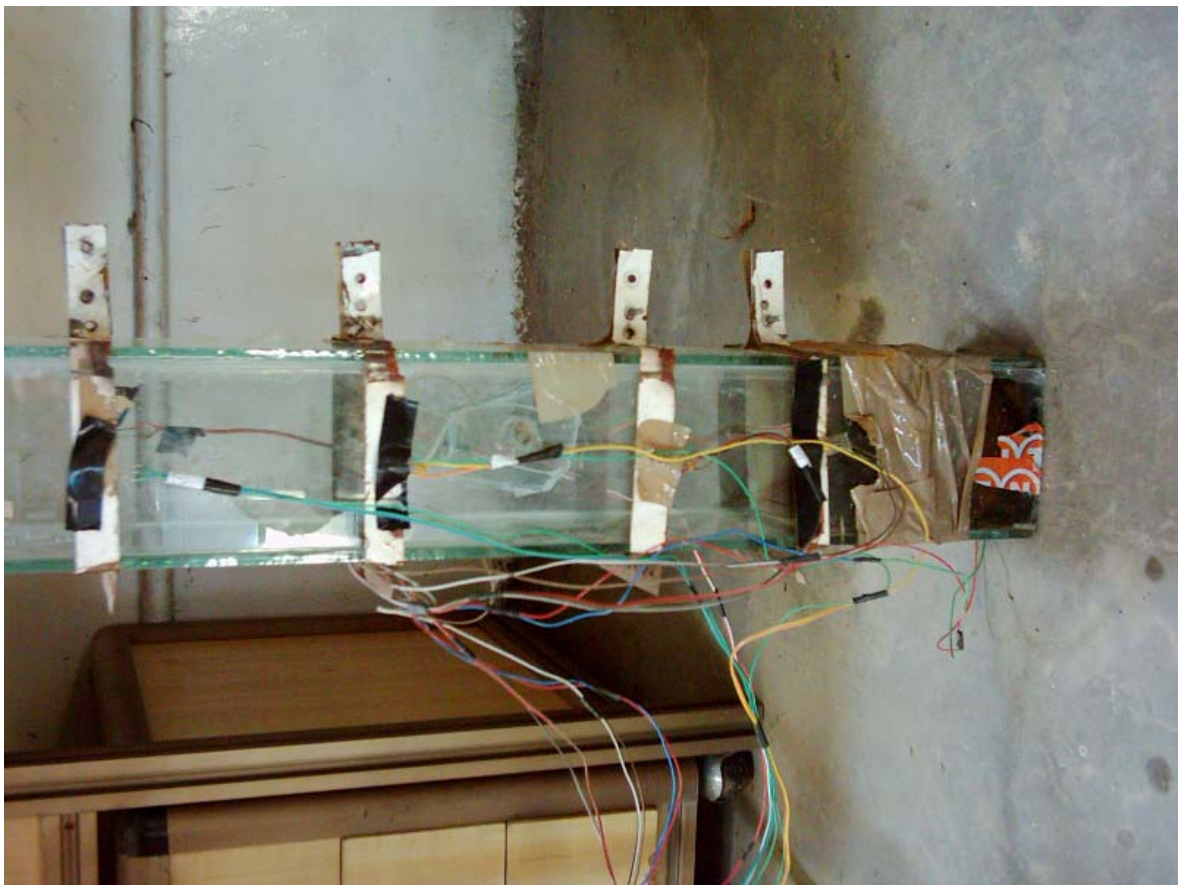

Figure (4-8) the plates used to hold the IR Transmitter-Receiver couples.

Figure (4-10) the structure for mounting the lunch device vertically.

Figure (4-1) the system of experiment.

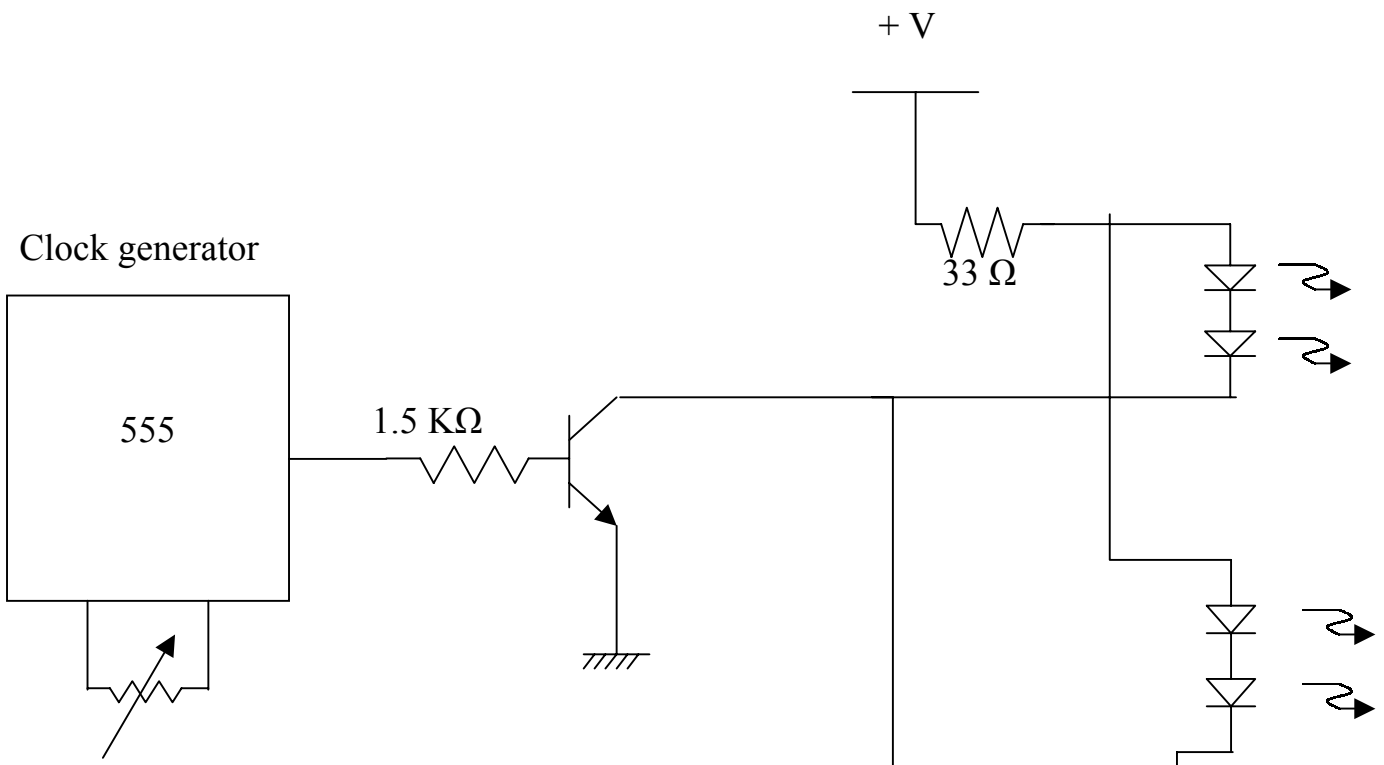

Figure (4-4) IR transmitter

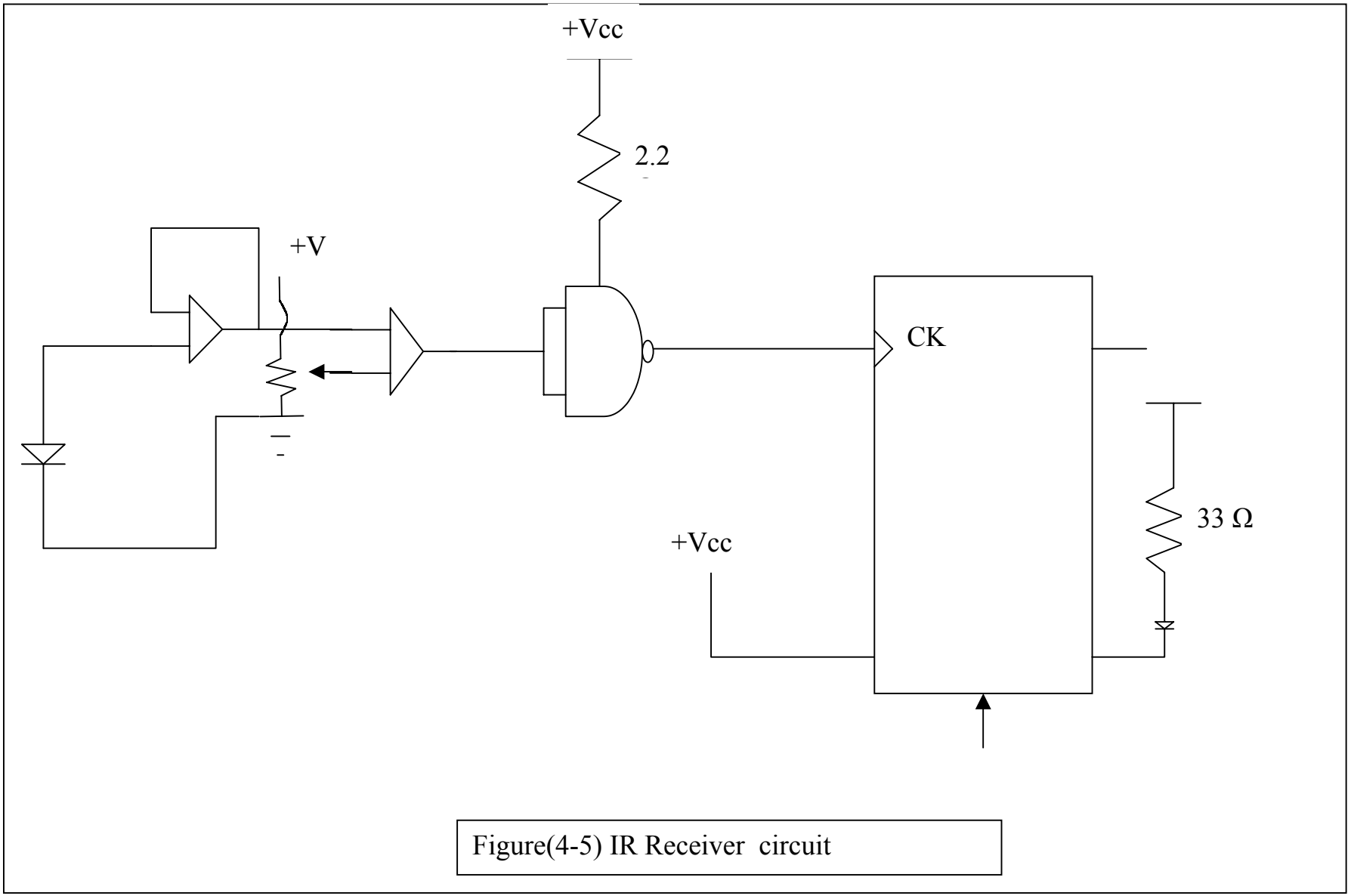

Figure(4-5) IR Receiver circuit

References

[1] Anderson, J., ”Fundamentals of Aerodynamics” McGraw-Hill 1991.

[2] A.N. Pavlov, s.s.sazhin, R.p. fedorenko , M.R. Heikal “Aconservative finite difference method and its application for the analysis of atransient flow around asquare prism “ International Journal of Numerical methods for heat and fluid flow “ vol.10 No.:2000, pp. 6-46.

[3] Arnal, M.P. , Goering , D.J. and Humphrey , J.A.C. (1991) “vortex shedding from a bluff body on a sliding wall” , J. fluid Eng . vol. 113, pp. 384-98 .

[4] Blake , R.W. (1981) “Influence of pectoral fin shape on thrust and drag in labriform locomotion “, Journal of zoology London , 194,53-66

[5] Clift , R., Grace , J.R. and weber , M.E. (1978) “Bubbles , Drops , and particles” , Academic press , sun Diega, CA.

[6] Chven- Yenchow “ An lutroduction to computional fluid Mechanics” John wiley and sons, Inc. 1979.

[7] Ciloudon and J. ZHANG “ measuring drag with out a force transducer a terminal velocity alloy” 2002 British. Ecological society.

[8] Douglas – Gasiorek . swaffield “ fluid Mechanics” second edition pitman .

[9] Davis , H.W. and Moore , E.F. (1982) “A numerical study of vortex shedding from rectangles” ,J. fluid Mech., vol. 119,pp.795-803

[10] Davis, W. Moor , E.F. and prcirtell, L.P.(1984) “A numerical experimental study of confined flow around rectangular cylinder” , phys. Fluid , vol. 27, pp.46-59 .

[11] F.W. Roos; W.W. willmarth , AIAA fournall 9, 285 (1971) .

[12] Fredrick J. Keller,W. Edeward Gettys, Malcom J. Skove,”Physics” Second Edition ,Mggraw-Hill,Inc. pp143.

[13] G. Matijasl , and A.Glasnovic “ Measurement and Evaluation

of drag coefficient for setting of spherical particles in psevdoplastic fluids" Accepted : 31.1.2001, university of Zagreb E-mail : gmatijs@ Pierre . Fkit.hr .

[14] Gal , J.M. and Bloke , R.W. (1987) hydrodynamic drag of two frogs species ; hymenochirus boettgcri and Rana pipiens . Canadian Journal of Zoology 65,1085-1090.

[15] Internet – "Drag measurement of cylindrical bodies".

[16] Johna. Roberson and Clayton- T.CR. "Engineering fluid mechanics" Washington state university, Pullman. Houghton Mifflin. Company.

[17] J.F. Douglas and R.D.Matthews. 3d edition "solving problems in fluid mechanics" volume2 Longman.

[18] Joseph B. Franzini, E.johon finnemore " Fluid mechanics with Engineering applications" McGraw-Hill.

[19] J.S. Mcnown, H.M.Lee, M.B. McPherson, and S.M.Enge2, "Influence of boundary prcximity on the drag spheres" proc. 7th intern . Appl .Mech. , 1948.

[20] J.L. Meriam and L.G.Kraige "Dynamics" 1987 2nd edition volume 2 .

[21] K.L. Kumar " Engineering fluid mechanics" 1997 Evrasia publishing house (p) LTD.

[22] Kilgore , R.A. and D.A. Dress "The application of cryogenics of high reyndds- numbers testing in wind tunnels" part2 . Development and application of the cryogenic wind tunnel concept , cryogenics , vol.24, no.9, September 1984 .

[23] Kue , S.S. (1972) , computer application of numerical methods , Addison – wevey , Reading , Mass.E.

[24] Kondo , N. and yamada , S.(1985) "Third-order upwind finite element computation of the incompressible navier- stokes

equations –part1 . Computation of flow around rectangular cylinders", compute methods Appl . Mech. Engrg, vol.127, pp. 87-97.
[25] Li, G. and Humphrey , J.A.C. (1995) "Numerical modeling of confined flow past a cylinder of square cross – section at various orientation" , Int. J. Numer. Methods fluid , vol. 20, pp. 1215-36 .
[26] Lamb, H. (1932) " Hydrodynamics" sixth edition , Cambridge university press , Cambridge , England (616, pp.105-324 .
[27] Mauricel . Albrtsson , James R.Barton , Anddary B.S.Mone "Fluid mechanics for engineers" prentice – Hall , INC.
[28] ME 224 Lab 6 "viscosity measurement" "IBM- pc in laboratory" by BG. Thomoson and A.F.Kuckes, ch.7.
[29] N.Mordant and J.F. pinton "velocity measurement of a setting sphere" The European physical journal B-2000 .
[30] Okajima, A., Ueno, H. and Sakai, H. (1992) "Numerical simulation of laminar and turbulent flow a round rectangular cylinders" Int. J. Numer. Methods fluid, vol. 15. pp.999-1012.
[31] Sohanker, A. Norberg, C. and Davidson, L.(1998) " Lout Reynolds- number flow a round a square cylinder at incidence: study of block age , onset of vortex shedding and out let boundary condition" , Int. J. Numer. Methods fluid, vol. 26, pp.39-56.
[32] Sighard F.Hoerner. "Fluid dynamic drag" practical information on Aerodynamic drag and Hydrodynamic resistances 1958 .
[33] Webb, P.W. (1975) " hydrodynamics and energetic of fish propulsion" Bulletin of fisheries research board of Canada 190, 1-159 .
[34] White , F.M. (1991) "viscous fluid flow" 2nd edition . Mc Graw hill, Newyork.
[35] Wissink, J.G. (1997) " DNS of 2D turbulent flow a round a square cylinder", Int. J.Numer. methods fluid, vol.25, pp.51-62.

[36] Victor L.streeter, E.Benjan in wylie. “Fluid mechanics” civil and mechanical engineering series . McGraw- Hill book company .pp.173.
[37] Vogel, S. (1983) “How much air passes through a silkmoths antenna? Journal of insect physiology 29, 596-602.
[38] Zhang .L.W., Tafti, D.K., Najjar, F.M.and Balachander, S.(1997) “computations of flow and heat transfer in parallel – plate fin heat
exchanges on the CM-5 : effect of flow unstediness and three – dimensionally”, Int. J. Heat . transfer, vol.40, pp. 1324-41.
[39] Xi, G.N., Hagiwara. Y.And Suzuki, K. (1995), “ Flow instability and augmented heat transfer of fin arrays”, J.Enhanced heat transfer, vol. 2,
pp.87-32.

الخلاصة

يهدف البحث إلى تصميم و بناء جهاز لقياس معامل الإعاقة للأجسام حرة الحركة و المعجلة في أوساط موائع مختلفة و لأشكال مختلفة.

تمت دراسة أربع عوامل رئيسية مؤثرة في حركة الجسم الساقط و هي الشكل حيث أخذت (الكرة،الاسطوانة) ،الأبعاد (0.8_15 mm) لكرات مصنوعة من الصلب الكاربوني و كرات زجاجية (0.5-20 mm) وللاسطوانات بأبعادl/d (2.5,4، 1.375، 1.444، 1.54، 1.33,3.3) ولأجسام مختلفة الكثافة، كما تم دراسة تأثير تغير الوسط(الماء،الهواء).

و من النتائج العملية تم الحصول على علاقة تغير السرعة بالنسبة للإزاحة حيث تم حساب معامل الإعاقة بعد الحصول على السرعة الثابتة(terminal velocity) من الجزء العملي للأجسام حرة السقوط. و عن طريق ذلك تم الحصول على علاقات معينة ما بين ال (Reynolds number) و معامل الإعاقة . و بعد مقارنة النتائج التي تم الحصول عليها من الجانب العملي و جدت أنها مقاربة للنتائج التي تم الحصول عليها من الجانب النظري للسرعة الثابتة. (terminal velocity)

أما بالنسبة لمعامل الإعاقة فقد كانت النتائج التي تم الحصول عليها من الجانب العملي مقاربة جداً للنتائج التي تم الحصول من المصدر.[16]

تصميم و تنفيذ منظومة قياس معامل الإعاقة الايرودينامكية

رسالة

مقدمة إلى كلية الهندسة في جامعة النهرين

و هي جزء من متطلبات نيل درجة ماجستير علوم في الهندسة الميكانيكية

من قبل

المهندس

حيدر حسن عبد بالة

(بكالوريوس هندسة ميكانيكية2001)

و ذلك في

شهر ربيع الثاني 1425 هـ

الموافق حزيران 2004 م